MedCrave
Step into the World of Research

Aeronautics and Aerospace Open Access Journal

Research Article

Open Access

CrossMark

Defect characterization of electron beam melted Ti-6Al-4V and Alloy 718 with X-ray microtomography

Abstract

Electron beam melting (EBM) is emerging as a promising manufacturing process where metallic components are manufactured from three-dimensional (3D) computer aided design models by melting layers onto layers. There are several advantages with this manufacturing process such as near net shaping, reduced lead times and the possibility to decrease weight by topology optimization, aspects that are of interest for the aerospace industry. In this work two alloys, Ti-6Al-4V and Alloy 718, widely used within the aerospace industry were investigated with X-ray microtomography (XMT), to characterize defects such as lack of fusion (LOF) and inclusions. It was furthermore possible to view the macrostructure with XMT, which was compared to macrostructure images obtained by light optical microscopy (LOM). XMT proved to be a useful tool for defect characterization and both LOF and un-melted powder could be found in the two investigated samples. In the EBM built Ti-6Al-4V sample high density inclusions, believed to be composed of tungsten, were found. One of the high-density inclusions was found to be hollow, which indicate that the inclusion stems from the powder manufacturing process and not related with the EBM process. By performing defect analyses with the XMT software it was also possible to quantify the amount of LOF and un-melted powder in vol%. From the XMT-data meshes were produced so that finite element method (FEM) simulations could be performed. From these FEM simulations the significant impact of defects on the material properties was evident, as the defects led to high stress concentrations. It could moreover, with FEM, be shown that the as-built surface roughness of EBM material is of importance as high surface roughness led to increased stress concentrations.

Keywords: X-ray tomography, Ti-6Al-4V, Alloy 718, defects and electron beam melting

Volume 1 Issue 3 - 2018

Magnus Neikter,[1] Fredrik Forsberg,[1] Robert Pederson,[2] Marta-Lena Antti,[1] Pia Åkerfeldt,[1] Simon Larsson,[1] Pär Jonsén,[1] Geraldine Puyoo[3]

[1]Luleå University of Technology, Sweden
[2]University West, Sweden
[3]GKN-Aerospace Engine Systems, Sweden

Correspondence: Magnus Neikter, Luleå University of Technology, 971 87 Luleå, Sweden, Email magnus.neikter@ltu.se

Received: April 07, 2018 | **Published:** May 18, 2018

Introduction

In order to apply additive manufacturing (AM) for manufacturing of components for the aerospace industry a number of requirements need to be fulfilled, especially for parts that have critical functions for the overall performance. Even though AM has a large global interest today, there are still many uncertainties and process-/material related parameters that lack enough knowledge and understanding before AM can be widely adopted for aerospace components. Some of these variables include mechanical properties[1–3] and their relationship to process parameters,[4,5] defects[6,7] etc. An aerospace driven research focus is also repeatability,[8] which means that one component manufactured in one AM machine should become exactly the same, or at least similar enough so that all necessary requirements are fulfilled, as if the same part was built in another machine of the same type. This has been realized to be difficult to achieve, especially for some AM processes where process complexity involves numerous variables. This is not necessarily only a disadvantage, the complexity with a number of variables can also be considered an advantage because it enables the flexibility to vary process parameters in different ways, depending on part geometry, material etc. and still manage to get the required end result. Two of the most important parameters to keep track of are temperature distribution and dimensional control.

AM is regarded as a beneficial manufacturing process over conventional manufacturing processes, when high complexity and low lot sizes are wanted.[9] Increased complexity and topology optimization make it possible to decrease the weight, remove assembly features, integrate mechanical functions, which are goals for aerospace designers.[10,11] One example of a highly complex structure that can be manufactured with AM is the honeycomb structure that could even include internal cooling channels.[11] Compared to other industrial sectors low lot sizes is a matter within the aerospace sector. This fact renders AM as a competitive option because the cost is similar whether one or several components are manufactured. In order to be able to qualify AM for manufacturing of critical applications more standards are needed to facilitate the qualification process. For competitiveness increased manufacturing speeds in most AM processes are needed, because conventional manufacturing processes can manufacture parts with higher rates. Normally some type of post processing of AM parts are needed, such as hot isostatic pressing (HIP)[4,6] to close pores and improve the mechanical properties and machining to obtain acceptable surface conditions. The need of post processing leads to decreased manufacturing speeds and higher costs. There are several different AM processes available and one promising AM process is electron beam melting (EBM) as it offers near net shape production, even for complex geometries, with little material waste which enables large weight saving possibilities.[12] EBM uses an electron beam as energy source to melt a powder bed and the chamber, in which the building is conducted, is kept at an elevated temperature throughout the build, which reduces the residual stresses compared with other competing powder bed processes.

Ti-6Al-4V and Alloy 718 are two alloys that are widely used in

aerospace applications. Ti-6Al-4V amounts to 80% of the total titanium alloys volume used within the aerospace sector,[13,14] whereas Alloy 718 is the most used Ni-based alloy within e.g. GE aircraft engines,[15] being an important alloy for rotating parts and at temperatures exceeding titanium's limit. AM of titanium has many advantages compared to conventional manufacturing because titanium is regarded as an expensive material compared to e.g. steel. The high production price for conventional manufacturing is partly due to that up to 80%[16] of the titanium is machined away and due to titanium's high affinity to oxygen making it a complicated metal to work with. If titanium is exposed to oxygen at high temperatures an oxide layer called α-case is formed, which reduces the mechanical properties.[17] The problem with titanium's affinity to oxygen is no issue when using EBM because the manufacturing takes place in vacuum. One of the main reasons for using titanium is that this metal has low density while having good mechanical properties giving it a high specific strength.[13,18] Titanium is furthermore a good choice for use in harsh environments as it has good corrosion resistance in most environments. In EBM, along with other AM processes, there are several types of defects that can form during the building process, such as lack of fusion (LOF), porosity and inclusions. LOF could for instance be caused by an insufficient amount of applied energy needed to melt the material. Porosity could as an example be caused by entrapped gas e.g. argon gas, while inclusions could arrive from various sources e.g. cross contamination. Previous work[6,19,20] has shown that defects like LOF present in AM can degrade the mechanical properties dramatically. Wycisk et al.[21] analyzed the effect of defects on fatigue properties and found that variations in fatigue properties to be the same for consistent defects, whereas a large variation was observed for different defects, their size and location. Anisotropy is another topic that has been reported for additive manufactured titanium,[22,23] leading to different mechanical properties in different loading directions.

In order to characterize microstructure and defects in AM materials it is common to make sample preparations, like cutting, grinding, polishing, etching etc., followed by microscopy evaluation. This type of characterization is time consuming and not completely accurate as only a part of the sample can be investigated and some defects might be missed. Furthermore, the sample of interest is destroyed in the process. A possible complement to this is to use X-ray microtomography (XMT)[24,25] which is a non-destructive characterization method that is used for obtaining high resolution 3D images of the investigated material. During the past 10-15 years XMT has become a popular tool for quantitative studies of various materials, including geological, biological, pharmaceutical and engineering materials.[26–29] XMT offers unique possibilities, where the high-resolution 3D image is an accurate map of the density and element distribution.[30] From the acquired 3D data, it is possible to make a quantitative characterization of the internal features (voids, cracks, grains, fibers etc.). Quantities such as porosity, volume fraction of phases and features, and grain size distribution, can be calculated using 3D image analysis.[26] Porosity of materials has traditionally been measured by Archimedes principle where the material is immersed in water and with the known density of water and the material, the porosity can be calculated. With XMT this porosity can be measured digitally, with high accuracy. In the last 40 years XMT has been used within the medical field with typical resolutions of 0.3mm,[31] but today with increased resolution it is also an interesting characterization technique in materials science where it is a powerful tool for e.g. detecting defects. The images are based on density distribution of the investigated material and one scan is composed of many X-ray projection images that are captured at equal angles of the sample, while the sample makes one full rotation. These images are then constructed into a 3D image by using tomographic reconstruction software. The XMT method can be used in both larger synchrotron facilities[30,31] and smaller in-house instruments.[32] Apart from direct analysis of the XMT data it is also possible to use the data to form authentic finite element models (FEM) of the sample, including the defects, for further analysis using FEM-software.[33] The FEM is the most developed and used numerical method based on continuum mechanics modelling, a constitutive relation for the actual material is described and the governing equations are solved.[33] The strength of the FEM is the many possibilities to study different mechanical and physical events. Also simple models can give interesting information on load and stress events and their consequences.

The aim of this work has been to show typical defects that are present in as built EBM Ti-6Al-4V and Alloy 718. These defects have furthermore been quantified and their distributions in the samples have been analyzed. The effects of the defects on mechanical properties are discussed in relation to already published results and the defect distribution is linked to process parameters.

Experimental method

Material and sample preparation

The Ti-6Al-4V sample was built in an Arcam Q20 machine while the Alloy 718 sample was built in an Arcam A2x machine. The height of the titanium sample was 30mm while the diameter ranged from 6-10mm (the titanium sample was a tensile bar with the bottom being 10mm in diameter). Both the samples were built with the process parameter contouring. The Alloy 718 was one quarter of a cylindrical sample, with the radius 5mm. The height of this sample was 28mm. Both the samples were printed in a vertical position in the building chambers. None of the samples received any post heat treatment or HIPing (hot isostatic pressing). Prior to the XMT analyze no sample preparation was needed as XMT is a non-destructive analyzing method. Prior to the microstructure characterization the titanium sample was cut perpendicular to the layers, so that the prior β grains could be revealed. The Alloy 718 sample was cut so that one quarter of the sample remained for the XMT analyze (otherwise it would be too thick for the X-rays). Parts of the two samples were then embedded in Bakelite followed by grinding and polishing according to conventional polishing methods for titanium and Alloy 718 samples. The titanium sample received an etching with Kroll's etchant according to ASTM Standard E 407 (192) and the Alloy 718 sample was etched with Kalling's etchant according to ASTM Standard E 407 (95).

Method

The two samples were scanned at the X-ray microtomography lab at Luleå University of Technology, Luleå, Sweden, using a Zeiss Xradia 510 Versa (Carl Zeiss X-ray Microscopy, Pleasanton, CA, USA). This imaging system provides flexibility with high resolution (down to <0.7μm spatial resolution and <70nm achievable voxel) and high contrast capabilities. The maximum tube voltage and power of the instrument is 160kV and 10W, respectively, which is sufficient to penetrate and scan a homogeneous cylindrical Ti-sample (density 4.5g/cm^3) of approximately 12mm diameter. The equivalent diameter for a nickel based sample such as Alloy 718 (density 8.9g/cm^3) is approximately 6mm. However, this is only approximate numbers and should therefore be considered as guidelines. The ZEISS Xradia 510

Citation: Neikter M, Forsberg F, Pederson R, et al. Defect characterization of electron beam melted Ti-6Al-4V and Alloy 718 with X-ray microtomography. *Aeron Aero Open Access J.* 2018;2(3):139–145. DOI: 10.15406/aaoaj.2018.02.00044

Versa system is also referred to as a 3D X-ray microscope (XRM) and has multiple detector objectives to enable imaging of the sample at a number of resolutions and field of view pairings, analogous to a light microscope. The Ti-6Al-4V sample was scanned two times using different objectives and scanning settings. The first scan, S1, is a large field of view (FOV) scan that covers the full cross section of the sample, with spatial resolution 8.23μm. The second scan, S2, is a local tomography scan, carried out with the spatial resolution 4.78μm. The third scan, S3, is a FOV scan in the mid-section with a spatial resolution of 11.31μm. The Alloy 718 sample was scanned with large FOV settings. This scan, denoted S4, was carried out with the spatial resolution 9.07μm. The full set of scanning parameters (FOV, spatial resolution, detector objective, voltage, power, exposure time, number of projections and the total scan time) is given in Table 1. 3D visualization and quantitative analysis of the microstructure in the AM samples were obtained using Dragonfly Pro software (ORS).

Table 1 Overview of the scan settings that were used for the four scans S1-S4

Scan	Spec	FOV (mm)	Res. (μm)	Obj.	Voltage (kV)	Power (W)	Exp. (s)	Proj.	Scan time (h)
S1	Ti-6Al-4V, top, FOV	8.42	8.23	0.4x	140	10	8	1601	5
S2	Ti-6Al-4V, top, local	4.82	4.78	4x	140	10	1	2201	2
S3	Ti-6Al-4V, mid, FOV	11.58	11.31	0.4x	150	10	6	1601	4
S4	Alloy 718	9.28	9.07	0.4x	160	10	12	1601	6

Mesh generation for FE-modelling was carried out using ScanIP software (Synopsys/Simpleware). For the microstructural characterization of both the Ti-6Al-4V and Alloy 718 samples a Nikon eclipse MA200 LOM was used. The software that was used for the LOM was NIS Elements BR that allows the user to take both macroscopic and high magnification (1000 times) images for distinguishing microstructural features. For the overview images several images were stitched together.

Finite element modelling

From the XMT measurements, finite element meshes were created for the Ti-6Al-4V and Alloy 718 samples. In order to study how defects in the samples affect the stress distributions, two finite element models were created for each sample. In the first model, all internal defects were included and in the second model, all internal defects were artificially removed. A quasi-static uniaxial displacement of 0.1mm in compression was simulated for the two samples. The non-linear finite element software LS-DYNA version R10.0[34] was used for the numerical simulations. For the finite element discretization of the samples, volume averaged 1-point nodal pressure tetrahedron elements were used. The finite element mesh of the Ti-6Al-4V sample with internal defects included had approximately 9.1 million elements, and the mesh with internal defects removed had approximately 5.6 million elements. For the Alloy 718, the mesh including internal defects had approximately 2.1 million elements, and the mesh with removed internal defects had approximately 1.8 million elements. More elements were required to accurately resolve the defects, hence the difference in number of elements between the models. Furthermore, the Ti-6Al-4V sample required more elements because it had a larger volume compared to the Alloy 718 sample. The height of the samples that was modelled was 7.1mm for Alloy 718, and 5.7mm for Ti-6Al-4V. A linear-elastic constitutive model was used to represent the Ti-6Al-4V and Alloy 718, and the elastic material parameters that were used are presented in Table 2.

Table 2 Elastic material parameters for Ti-6Al-4V and Alloy 718

	Ti-6Al-4V[35]	Alloy 718[36]
Young's modulus (GPa)	113.8	200
Poisson's ratio	0.342	0.294
Density (g/cm^3)	4.43	8.19

Results and discussion

Microstructures

Figure 1 shows the microstructures of the Alloy 718 (Figure 1A) and the Ti-6Al-4V samples (Figure 1B). The microstructure of EBM manufactured Alloy 718 in as built condition consists of a gamma phase matrix with a columnar structure. Delta phase with needle like morphology and MC carbides (mainly NbC) are distributed in the matrix. The main strengthening precipitate in Alloy 718 is gamma double prime which is also present in the as built condition. The distribution of all the secondary phases is heterogeneous and depends on the part geometry, especially the height and thickness. For Ti-6Al-4V, β grains are formed above the beta transus temperature and these prior β grains grow epitaxially with a β<100> crystal growth[37,38] through the layers towards the temperature gradient direction.[39,40] When the temperature decreases below the β transus temperature α laths start to form from the β grain boundaries, and from within the grains depending on cooling rate. The microstructure of the present Ti-6Al-4V EBM sample was determined to be of basket weave type, where entangled α laths is the characteristic feature. When cooling rate is slow enough, α phase will nucleate and grow in the β grain boundaries, making the β grains easy to distinguish. Epitaxial growth of grains perpendicular to the layers was seen in both materials.

The prior β grains in the Ti-6Al-4V sample can clearly be seen in Figure 2, both in the macrostructure from XMT (Figure 2A) and in the macrostructure from LOM (Figure 2B). When comparing these two

characterization techniques it can be concluded that both techniques show these prior β grains, although for LOM the grain boundaries appear more clearly. For XMT it was not possible to investigate the microstructure of the investigated material; however it gives a full 3D representation, which is something that is important when there are local variations, variations that could stay undetected when investigating in 2D, such as with LOM.

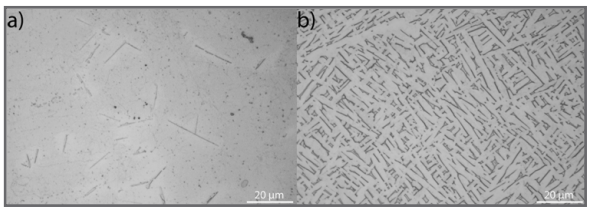

Figure 1 (A) Microstructure of Alloy 718, (B) Ti-6Al-4V. The microstructure of Alloy 718 is composed of a gamma phase matrix with needle like δ phase and MC carbides, while the microstructure of the Ti-6Al-4V sample is basket weave, where the intertwined α laths is a characteristic feature.

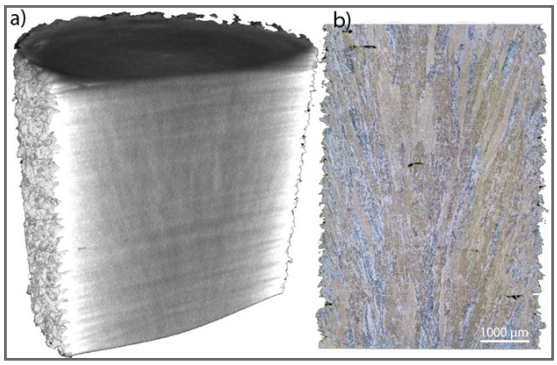

Figure 2 (A) the macrostructure from the XMT image and (B) the macrostructure as seen from the LOM. In both characterization methods the prior β grains growing epitaxially from one layer to another can be seen.41

Defects

In AM there are mainly three different defects that can be present in the build, LOF, porosity and inclusions. In general, pores are considered as spherical defects, LOF non-symmetrical defects and the inclusions are defects exhibiting different chemical composition than the base metal. All these three defects were found in the two investigated materials. LOF and porosity are known to be detrimental to the mechanical properties.[6,19] Cao et al.[7] investigated process parameters that altered the amounts of porosity and a clear correlation between the amount of porosity and tensile strength was observed. The process parameters with low amount of porosity had better tensile properties than material with high amount of porosity. Cao et al.[7] also investigated the effect of orientation of the defects on the tensile properties, concluding that elongated defects parallel to the layers reduce the tensile properties if a load perpendicular to the layers is applied, due to that the defects are opened up. Whereas if a load parallel to the layers is applied the crack is closed. LOF is mainly formed in the interface between layers i.e. parallel to the layers, thus if load is applied parallel or perpendicular to the layers anisotropic behavior occurs, thus partly explaining the anisotropic behavior that is observed in AM.[7,22] Qui et al.[42] and Kobryn et al.[6] also supported this reasoning of defects impact on fracture elongation.

In Figure 3A & Figure 3B two different digital slices of the Alloy 718 sample are shown and the typical appearance of defects in the XMT images are distinguished by a difference in contrast as e.g. highlighted by black arrows in Figure 3B. In this case the LOF shown by the left black arrow in b) is parallel to the layers, thus it would according to the theory discussed previously decrease the tensile properties if load would be applied perpendicular to the layers, while not affecting a loading parallel to the layers.

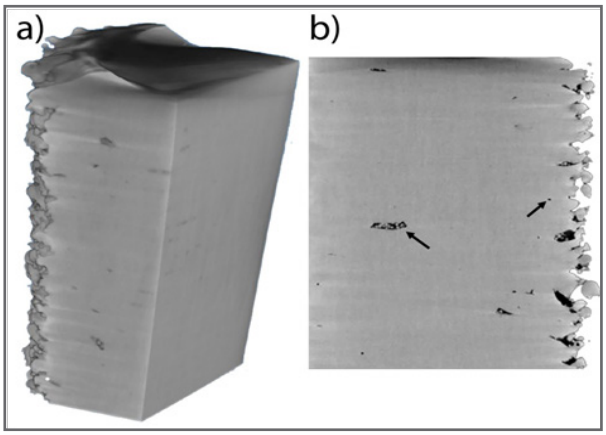

Figure 3 XMT images of the Alloy 718 sample. (A) An overview image showing different sections of the material in 3D perspective. (B) A section of the material exhibiting several defects which are represented by a contrast difference (black spots) in the image, two defects being highlighted by black arrows.

In order to evaluate the defects more carefully, defect analyzes of the two samples were carried out and the result is shown in Figure 4. The green color signifies cavities in the material i.e. LOF or pores and the red color signifies spherical shapes with a different density, compared to the cavities, which in this case could be related to un-melted powder due to LOF. In Figure 4B it is clearly shown that the un-melted powder (red shapes) is present within irregular cavities, which is related to the incomplete melting of powder i.e. LOF. In Table 3, the amount of cavities and un-melted powder for the evaluated volume of the materials is shown for Ti-6Al-4V and Alloy 718. Noteworthy is the difference in the amount of cavities when comparing the two materials, where Alloy 718 has more defects. Moreover, the distribution of defects seems to be higher close to the surface while the bulk has lower amounts of defects. The higher defect level near the surface compared to the bulk could be explained by the process parameter "contouring"[43,44] that creates an edge effect leading to an increased amount of defects close to the contour line. Contouring is used for improving surface quality and is done by melting the contour, prior to the hatching phase, and is normally performed in two steps, inner and outer contouring. According to Smith et al.[4] the dimensional accuracy of EBM can be improved by not using contouring and by reducing the beam energy density by increasing the beam speed. The drawbacks with this are on the other hand an increased amount and size of porosity in localized regions. The defects could however be closed by performing HIP treatment,[4,6] which is a process that heat the material to about 900°C in high pressure atmosphere. The combination of elevated temperature and the high pressure leads to those vacancies are closed. It is however desired not to perform this post treatment as it increases the manufacturing time and cost.

Two inclusions were found in the investigated Ti-6Al-4V sample and in Figure 5A an XMT view of an inclusion is shown. The inclusion

is distinguished in the XMT by a different density contrast, in this case the inclusion shows high intensity i.e. bright particle, see white arrows.

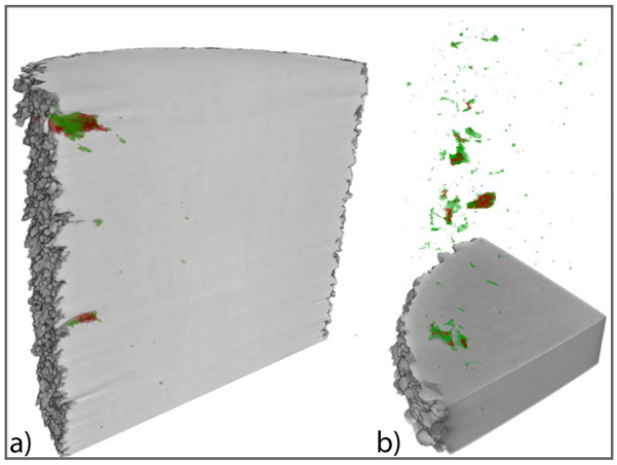

Figure 4 (A) the Ti-6Al-4V sample and (B) the Alloy 718 sample. The green color signifies porosity while the red signifies spherical particles.

Table 3 The amount of cavities (porosity and LOF) and un-melted powder for the two samples

	Ti-6Al-4V	Alloy 718
Sample volume (mm^3)	172.8	130.7
Cavities (vol%)	0.056	0.121
Un-melted powder (vol%)	0.022	0.026

In Figure 5 an inclusion is shown, at low (b) and high (c) magnification. Its diameter was measured to be approximately 150µm. This type of inclusions could originate from various sources e.g. from storage conditions, cross contamination from different powders and the actual powder production. The tomography instrument used is not equipped with any spectroscopy possibilities and hence it was not possible to determine the exact element of the inclusion. However, the high intensity makes it possible to conclude that it is a high-density inclusion. One plausible element is thus tungsten, an element that has been verified to exist in additive manufactured titanium in other studies.[23] During the powder production a tungsten filament was utilized for melting the material. Thus a tungsten inclusion could for instance come from this filament, as it has been reported that the tungsten filament can wear out and emit such small particles.[18] So, a possible reason for this "donut"-shaped inclusion in Figure 5 could be that during the powder production, the high-pressure gas that is used somehow penetrated the liquid spherical powder creating this void. Tungsten filaments are also used to create the electron beam in the EBM machine, but the machine itself can be ruled out as the source of the inclusion due to the facts that the void is located in the center of the inclusion and that the machine is structured to prevent this to occur. So due to this it is thought that this inclusion comes from the powder production rather than from the EBM process itself. Tungsten inclusions are hard and brittle at low temperatures[45] and its high melting temperature will make it stay un-melted in liquid titanium and Alloy 718. Due to their brittle nature they can act as crack initiation sites leading to reduced mechanical properties. According to Brando et al.[23] the impact of these inclusions have a similar impact on the mechanical properties as LOF, thus being a highly unwanted feature in AM built material. In the Alloy 718 sample no high density inclusion was found.

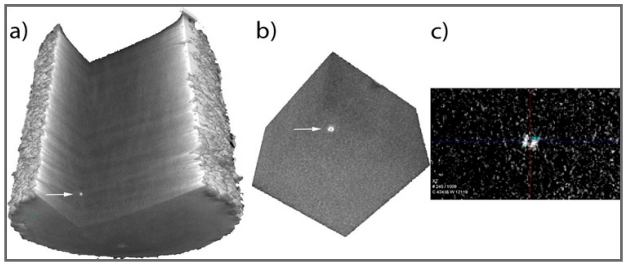

Figure 5 (A) Inclusion in Ti-6Al-4V shown in one out of many possible views by XMT. In these digital cuts only one high density inclusion is present, although more high-density inclusions can hide in other cuts. (B) and (C) show the high-density inclusion in different magnifications, (B) low and (C) high magnification. In both images it is seen that the particle has a cavity in the middle, giving it a "donut-shape". In the high magnification image (C), it was also possible to measure the radius of the particle to 76.9µm.

Finite element simulation

The distribution of the effective von Mises stress in the Alloy 718 and Ti-6Al-4V models were evaluated from uniaxial compression simulations. Figure 6A shows the position of the cross sections used. In Figure 6B one cross section from the Alloy 718 models without internal defects is shown, and Figure 6C shows the model with internal defects. The corresponding cross sections for the Ti-6Al-4V models are shown in Figure 7. The models where the defects were included resulted in the development of stress concentrations close to the defects. This is shown in Figure 6C and Figure 7C, where the defects in the interior of the samples appear as voids in the cross sections. Components that have large stress concentrations are more prone to initiation of cracks and premature fatigue failure. Figure 8 shows the distribution of the effective von Mises stress on the surface of the Alloy 718 and Ti-6Al-4V models. Stress concentrations were observed on the surfaces of both materials, giving a good indication of the severity of rough surfaces for the mechanical properties. Rough surfaces that result in stress concentrations will decrease the mechanical properties of a component. Due to the stress concentrations, the surfaces of the materials are prone to crack initiation thus decreasing the resistance to fatigue. This is in good correlation with Chan et al.,[46] who investigated the effect of surface roughness on the fatigue properties of EBM built Ti-6Al-4V. The conclusion of their study was that the roughness decreased the fatigue life time.

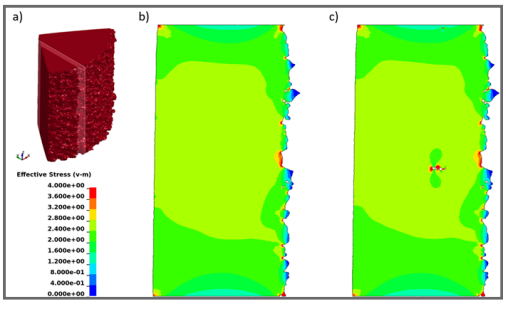

Figure 6 Finite element model of the Alloy 718 sample. (A) The position of the cross section used to study how internal defects affect the stress state in the sample during uniaxial compression. Cross sections (B) and (C) showing the effective von Mises stress after simulated uniaxial compression of the Alloy 718 sample, where (B) is without and (C) with internal defects. The impact of defects is shown as stress concentrations located at the interior void in (C). Stress concentrations could lead to crack initiation and eventually to premature material failure. The effect of the surface roughness is also visible as swift changes between high and low stresses.

Citation: Neikter M, Forsberg F, Pederson R, et al. Defect characterization of electron beam melted Ti-6Al-4V and Alloy 718 with X-ray microtomography. *Aeron Aero Open Access J.* 2018;2(3):139–145. DOI: 10.15406/aaoaj.2018.02.00044

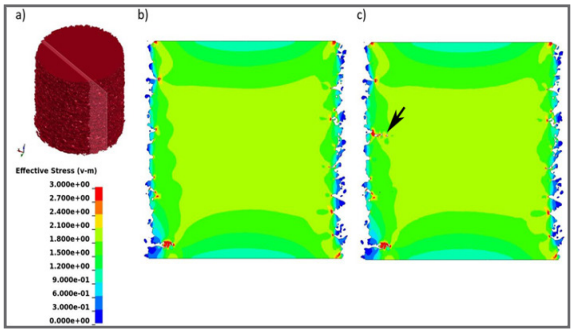

Figure 7 Finite element model of the Ti-6Al-4V sample (A) the position of the cross section used to study how internal defects affect the stress state in the sample during uniaxial compression. Cross sections (B) and (C) showing the effective von Mises stress after simulated uniaxial compression of the Ti-6Al-4V sample, where (B) is without and (C) with internal defects. The impact of defects is shown as stress concentrations located at the interior void in (C) (see black arrow). Stress concentrations could lead to crack initiation and eventually to premature material failure. The effect of the surface roughness is also visible as swift changes between high and low stresses.

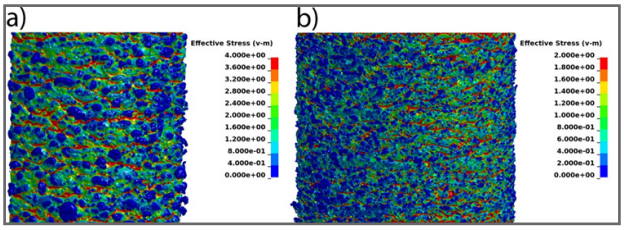

Figure 8 Stress concentrations of the Alloy 718 (A) and Ti-6Al-4V (B) samples from the surface point of view. The surface, with its high roughness, has many stress concentrations (red) combined with areas (blue) with no stress.

Conclusion

In this study XMT was used to detect small high-density inclusions and with XMTs high spatial resolution their size was determined to 150nm in diameter. With XMT it was furthermore possible to distinguish the macrostructure of Ti-6Al-4V in the form of prior β grains. As a defect characterization technique XMT was superior to conventional characterization including sample preparation combined with LOM, both in regard to time efficiency, reliability and being non-destructive. Moreover, it was concluded that as built EBM Ti-6Al-4V had a total of 0.078vol% defects (cavities and un-melted powder) in the material. For the EBM built Alloy 718 sample the corresponding amount was 0.147vol%. With the defect distribution analyze it was also shown that a majority of the defects were found closer to the surface, which from previous research has been correlated with the process parameter "contouring", which both the samples were built with. Characterizing the microstructure with the current XMT was not possible, apart from a macroscopic point of view. So if a thorough characterization is wanted one should first start with the XMT scanning as this technique is non-destructive, to identify features (e.g. defects) in three dimensions. Then once that is done LOM can be used to characterize certain regions that are of more interest and then in combination obtain a good overall characterization. From the finite element analysis both internal- and surface defects showed information on local stress concentrations and from the result it was shown that the defects lead to high stress concentrations, that consequently will lead to crack initiation sites and premature failure. By analyzing the result of the FEM simulations it was also evident of the necessity to have fine surfaces, as rough surfaces result in higher stress concentrations. These simulations clearly showed the severe impact that defects can have on the lifetime of components having these defects. FEM modeling is thus giving important information for evaluating future fatigue strength on AM products.

Acknowledgements

The author would like to thank GKN-Aerospace Engine Systems along with the "Graduate School of Space Technology", the EU funded project Space for innovation and growth" and "Nationellt rymdtekniskt forskningsprogram" for their financial support and contributions. Furthermore, thanks to Kempestiftelserna and LKAB for making it possible to run XMT at Luleå University of Technology.

Conflict of interest

The author declares that there is no conflict of interest.

References

1. Carroll BE, Palmer TA, Beese AM. Anisotropic tensile behavior of Ti–6Al–4V components fabricated with directed energy deposition additive manufacturing. *Acta Materialia*. 2015;87:309–320.
2. Rafi H, Karthik N, Gong H, et al. Microstructures and Mechanical Properties of Ti6Al4V Parts Fabricated by Selective Laser Melting and Electron Beam Melting. *J of Materi Eng and Perform*. 2013;22(12):3872–3883.
3. Sandgren HR, Zhai Y, Lados DA, et al. Characterization of fatigue crack growth behavior in LENS fabricated Ti-6Al-4V using high-energy synchrotron x-ray microtomography. *Additive Manufacturing*. 2016;12(Part A):132–141.
4. Smith CJ, Derguti F, Nava EH, et al. Dimensional accuracy of Electron Beam Melting (EBM) additive manufacture with regard to weight optimized truss structures. *J Mater Process Technol*. 2016;229:128–138.
5. Shi X, Ma S, Liu C, et al. Performance of High Layer Thickness in Selective Laser Melting of Ti6Al4V. *Materials*. 2016;9(12):975.
6. Kobryn PA, Semiatin SL. *Mechanical Properties of Laser-Deposited Ti-6Al-4V*. Austin: Proceedings of 12th Solid Freeform Fabrication Symposium; 2001. 186 p.
7. Cao S, Chen Z, Lim CVS, et al. Defect, microstructure, and mechanical property of Ti-6Al-4V alloy fabricated by high-power selective laser melting. *JOM*. 2017;69(12):2684–2692.
8. Lyons B. Additive manufacturing in aerospace: Examples and research outlook. *The Bridge*. 2014;42(1):1–13.
9. Frazier WE. Metal additive manufacturing: a review. *J of Materi Eng and Perform*. 2014;23(6):1917–1928.
10. Wong KV, Hernandez A. A review of additive manufacturing. ISRN Mechanical Engineering. 2012;208760:1–10.
11. Campbell I, Bourell D, Gibson I. Additive manufacturing: rapid prototyping comes of age. *Rapid Prototyping Journal*. 2012;18(4):255–258.
12. Dutta B, Froes FH. The Additive Manufacturing (AM) of titanium alloys. *Metal Powder Report*. 2017;72(2):96–106.
13. Lütjering G, Williams JC. *Titanium*. 2nd ed. Newyork: Springer; 2007. 442 p.
14. Henry SD. *Fatigue data book*. 1st ed. Materials Park, OH: ASM; 1995.
15. Schafrik RE, Ward DD, Groh JR. Application of alloy 718 in GE aircraft engines: past, present and next five years. *Superalloys*. 2001;718:625–706.

16. Gibson I, Rosen DW, Stucker B. *Additive manufacturing technologies*. New York: Springer; 2010. 19 p.
17. Boyer RR. An overview on the use of titanium in the aerospace industry. *Materials Science and Engineering: A*. 1996;213(1-2):103–114.
18. Donachie MJ. *Titanium: a technical guide*. 2nd ed. USA: ASM international; 2000. 381 p.
19. Qiu C, Ravi GA, Dance C, et al. Fabrication of large Ti–6Al–4V structures by direct laser deposition. *Journal of Alloys and Compounds*. 2015;629:351–361.
20. Vilaro T, Colin C, Bartout J. As-fabricated and heat-treated microstructures of the Ti-6Al-4V alloy processed by selective laser melting. *Metall and Mat Trans A*. 2011;42(10):3190–3199.
21. Wycisk E, Solbach A, Siddique S, et al. Effects of defects in laser additive manufactured Ti-6Al-4V on fatigue properties. *Physics Procedia*. 2014;56:371–378.
22. Edwards P, O'Conner A, Ramulu M. Electron beam additive manufacturing of titanium components: properties and performance. *J Manuf Sci Eng*. 2013;135(6):061016.
23. Brando AD, Gerard R, Gumpinger J, et al. Challenges in Additive Manufacturing of Space Parts: Powder Feedstock Cross-Contamination and Its Impact on End Products. *Materials*. 2017;10(5):522.
24. Elliott JC, Dover SD. X□ray microtomography. *J Microsc*. 1982;126(2):211–213.
25. Flannery BP, Deckman HW, Roberge WG, et al. Three-dimensional X-ray microtomography. *Science*. 1987;237(4821):1439–1444.
26. Maire E, Withers PJ. Quantitative X-ray tomography. *International Materials Reviews*. 2014;59(1):1–43.
27. Stock SR. Recent advances in X-ray microtomography applied to materials. *International Materials Reviews*. 2008;53(3):129–181.
28. Lu S, Landis EN, Keane DT. X-ray microtomographic studies of pore structure and permeability in Portland cement concrete. *Mater Struct*. 2006;39(6):611-620.
29. Forsberg F, Mooser R, Arnold M, et al. 3D micro-scale deformations of wood in bending: synchrotron radiation μCT data analyzed with digital volume correlation. *J Struct Biol*. 2008;164(3):255–262.
30. Flannery BP, Deckman HW, Roberge WG, et al. Three-dimensional X-ray microtomography. *Science*. 1987;237(4821):1439–1444.
31. Maire E, Buffiere J, Salvo L, et al. On the application of X-ray microtomography in the field of materials science. *Advanced Engineering Materials*. 2001;3(8):539–546.
32. Slotwinski JA, Garboczi EJ, Hebenstreit KM. Porosity measurements and analysis for metal additive manufacturing process control. *Journal of research of the National Institute of Standards and Technology*. 2014;119:494–528.
33. Zienkiewicz OC, Taylor RL. *The finite element method: solid mechanics*. 5th ed. UK: Butterworth-heinemann; 2000. 476 p.
34. *LS-DYNA Keyword User's Manual*. USA: Livermore Software Technology Corporation; 2017.
35. *Materials data for Ti-6Al-4V*. USA: ASM Aerospace Specifications Metals Inc; 2017.
36. *Data sheet Alloy 718*. USA: Special Metals; 2017. 28 p.
37. Lancaster R, Davies G, Illsley H, et al. Structural integrity of an electron beam melted titanium alloy. *Materials*. 2016;9(6):470.
38. Antonysamy AA, Meyer J, Prangnell PB. Effect of build geometry on the β-grain structure and texture in additive manufacture of Ti6Al4V by selective electron beam melting. *Materials Characterization*. 2013;84:153–168.
39. Neikter M, Akerfeldt P, Pederson R, et al. Microstructural characterization and comparison of Ti-6Al-4V manufactured with different additive manufacturing processes. *Materials Characterization*. 2018.
40. Neikter M, Akerfeldt P, Pederson R, et al. Microstructure characterisation of Ti-6Al-4V from different additive manufacturing processes. *IOP Conf Ser: Mater Sci Eng*. 2017;258:012007.
41. Neikter M, Forsberg F, Lycksam H, et al. *Microstructure and defects in additive manufactured titanium: A comparison between microtomography and optical microscopy*. Sweden: 3rd International Conference on Tomography of Materials and Structures; 2017.
42. Qiu C, Ravi GA, Dance C, et al. Fabrication of large Ti–6Al–4V structures by direct laser deposition. *J Alloys Compounds*. 2015;629:351–361.
43. Fox JC, Moylan SP, Lane BM. Effect of process parameters on the surface roughness of overhanging structures in laser powder bed fusion additive manufacturing. *Procedia CIRP*. 2016;45:131–134.
44. Evren Y, Deckers J, Craeghs T, et al. *Investigation on occurrence of elevated edges in selective laser melting*. Belgium: Catholic University of Leuven; 2009. 13 p.
45. Lassner E, Schubert W. *Tungsten: Properties, Chemistry, Technology of the Element, Alloys, and Chemical Compounds*. 1st ed. Boston: Springer; 1999. 422 p.
46. Chan KS, Koike M, Mason RL, et al. Fatigue life of titanium alloys fabricated by additive layer manufacturing techniques for dental implants. *Metall and Mat Trans A*. 2013;44(2):1010–1022.

Citation: Neikter M, Forsberg F, Pederson R, et al. Defect characterization of electron beam melted Ti-6Al-4V and Alloy 718 with X-ray microtomography. *Aeron Aero Open Access J.* 2018;2(3):139–145. DOI: 10.15406/aaoaj.2018.02.00044